Title	J-GEM follow-up observations of the gravitational wave source GW151226
Author(s)	Yoshida; Michitoshi; Utsumi; Yousuke; Tominaga; Nozomu; Morokuma; Tomoki; Tanaka; Masaomi; Asakura; Yuichiro; Matsubayashi; Kazuya; Ohta; Kouji; Abe; Fumio; Chimasu; Sho; Furusawa; Hisanori; Itoh; Ryosuke; Itoh; Yoichi; Kanda; Yuka; Kawabata; S., Koji; Kawabata; Miho; Koshida; Shintaro; Koshimoto; Naoki; Kuroda; Daisuke; Moritani; Motohara, Yuki; Kentaro; Murata; L., Katsuhiro; Nagayama; Takahiro; Nakaoka; Tatsuya; Nakata; Fumiaki; Nishioka; Tsubasa; Saito; Yoshihiko; Terai; Tsuyoshi; Tristram; J., Paul; Yanagisawa; Kenshi; Yasuda; Naoki; Doi; Mamoru; Fujisawa; Kenta; Kawachi; Akiko; Kawai; Nobuyuki; Tamura; Yoichi; Uemura; Makoto; Yatsu; Yoichi
Citation	Publications of the Astronomical Society of Japan (2017), 69(1)
Issue Date	2017-02
URL	http://hdl.handle.net/2433/235004
Right	© The Author 2016. Published by Oxford University Press on behalf of the Astronomical Society of Japan. This is an Open Access article distributed under the terms of the Creative Commons Attribution License (http://creativecommons.org/licenses/by/4.0/), which permits unrestricted reuse, distribution, and reproduction in any medium, provided the original work is properly cited.
Type	Journal Article
Textversion	publisher

Publ. Astron. Soc. Japan (2017) 69 (1), 9 (1–12)
doi: 10.1093/pasj/psw113
Advance Access Publication Date: 2016 December 5

J-GEM follow-up observations of the gravitational wave source GW151226*

Michitoshi Yoshida,[1,†] Yousuke Utsumi,[1] Nozomu Tominaga,[2,3] Tomoki Morokuma,[4,5] Masaomi Tanaka,[5,3] Yuichiro Asakura,[6] Kazuya Matsubayashi,[7] Kouji Ohta,[7] Fumio Abe,[6] Sho Chimasu,[8] Hisanori Furusawa,[5] Ryosuke Itoh,[9,10] Yoichi Itoh,[11] Yuka Kanda,[9] Koji S. Kawabata,[1] Miho Kawabata,[9] Shintaro Koshida,[12] Naoki Koshimoto,[13] Daisuke Kuroda,[14] Yuki Moritani,[3] Kentaro Motohara,[4] Katsuhiro L. Murata,[15] Takahiro Nagayama,[16] Tatsuya Nakaoka,[9] Fumiaki Nakata,[12] Tsubasa Nishioka,[17] Yoshihiko Saito,[10] Tsuyoshi Terai,[12] Paul J. Tristram,[18] Kenshi Yanagisawa,[14] Naoki Yasuda,[3] Mamoru Doi,[4,19] Kenta Fujisawa,[20] Akiko Kawachi,[8] Nobuyuki Kawai,[10] Yoichi Tamura,[4] Makoto Uemura,[1] and Yoichi Yatsu[10]

[1]Hiroshima Astrophysical Science Center, Hiroshima University, 1-3-1 Kagamiyama, Higashi-Hiroshima, Hiroshima 739-8526, Japan
[2]Department of Physics, Faculty of Science and Engineering, Konan University, 8-9-1 Okamoto, Kobe, Hyogo 658-8501, Japan
[3]Kavli Institute for the Physics and Mathematics of the Universe (WPI), The University of Tokyo, 5-1-5 Kashiwanoha, Kashiwa, Chiba 277-8583, Japan
[4]Institute of Astronomy, Graduate School of Science, The University of Tokyo, 2-21-1 Osawa, Mitaka, Tokyo 181-0015, Japan
[5]National Astronomical Observatory of Japan, 2-21-1 Osawa, Mitaka, Tokyo 181-8588, Japan
[6]Institute for Space-Earth Environmental Research, Nagoya University, Chikusa-ku, Nagoya, Aichi 464-8601, Japan
[7]Department of Astronomy, Kyoto University, Kitashirakawa-Oiwake-cho, Sakyo-ku, Kyoto, Kyoto 606-8502, Japan
[8]Department of Physics, School of Science, Tokai University, 1117 Kita-kaname, Hiratsuka, Kanagawa 259-1292, Japan
[9]Department of Physical Science, Hiroshima University, 1-3-1 Kagamiyama, Higashi-Hiroshima, Hiroshima 739-8526, Japan
[10]Department of Physics, Tokyo Institute of Technology, 2-12-1 Ookayama, Meguro-ku, Tokyo 152-8551, Japan
[11]Nishi-Harima Astronomical Observatory, University of Hyogo, 407-2 Nishigaichi, Sayo-cho, Sayo, Hyogo 679-5313, Japan
[12]Subaru Telescope, National Astronomical Observatory of Japan, 650 North A'ohoku Place, Hilo, HI 96720, USA
[13]Department of Earth and Space Science, Graduate School of Science, Osaka University, 1-1 Machikaneyama-cho, Toyonaka, Osaka 560-0043, Japan
[14]Okayama Astrophysical Observatory, National Astronomical Observatory of Japan, 3037-5 Honjou, Kamogata, Asakuchi, Okayama 719-0232, Japan

[15]Department of Particle and Astrophysical Science, Nagoya University, Chikusa-ku, Nagoya, Aichi 464-8602, Japan
[16]Graduate School of Science and Engineering, Kagoshima University, 1-21-40 Korimoto, Kagoshima, Kogoshima 890-0065, Japan
[17]Department of Physics, Faculty of Science, Kyoto Sangyo University, Motoyama, Kamigamo, Kita-Ku, Kyoto, Kyoto 603-8555, Japan
[18]Mt John University Observatory, P.O. Box 56, Lake Tekapo 8770, New Zealand
[19]Research Center for the Early Universe, Graduate School of Science, The University of Tokyo, 7-3-1 Hongo, Bunkyo-ku, Tokyo 113-0033, Japan
[20]The Reseach Institute of Time Studies, Yamaguchi University, 1677-1 Yoshida, Yamaguchi, Yamaguchi 753-8511, Japan

[†]E-mail: yoshidam@hiroshima-u.ac.jp

[*]Based on data collected at the Subaru Telescope, which is operated by the National Astronomical Observatory of Japan.

Received 2016 October 3; Accepted 2016 November 5

Abstract

We report the results of optical–infrared follow-up observations of the gravitational wave (GW) event GW151226 detected by the Advanced LIGO in the framework of J-GEM (Japanese collaboration for Gravitational wave ElectroMagnetic follow-up). We performed wide-field optical imaging surveys with the Kiso Wide Field Camera (KWFC), Hyper Suprime-Cam (HSC), and MOA-cam3. The KWFC survey started at 2.26 d after the GW event and covered 778 deg^2 centered at the high Galactic region of the skymap of GW151226. We started the HSC follow-up observations from $\sim$12 d after the event and covered an area of 63.5 deg^2 of the highest probability region of the northern sky with limiting magnitudes of 24.6 and 23.8 for the *i* and *z* bands, respectively. MOA-cam3 covered 145 deg^2 of the skymap with the MOA-red filter $\sim$2.5 mon after the GW alert. The total area covered by the wide-field surveys was 986.5 deg^2. The integrated detection probability for the observed area was $\sim$29%. We also performed galaxy-targeted observations with six optical and near-infrared telescopes from 1.61 d after the event. A total of 238 nearby ($\leq$100 Mpc) galaxies were observed with a typical *I* band limiting magnitude of $\sim$19.5. We detected 13 supernova candidates with the KWFC survey, and 60 extragalactic transients with the HSC survey. Two thirds of the HSC transients were likely supernovae and the remaining one third were possible active galactic nuclei. With our observational campaign, we found no transients that are likely to be associated with GW151226.

Key words: binaries: close — black hole physics — gravitational waves — methods: observational — surveys

1 Introduction

A gravitational wave (GW) is a quadrupole wave of space-time distortion propagating with light speed. Strong GWs are emitted by violent gravitational disturbance induced by a coalescence between compact massive objects such as neutron stars (NSs) or black holes (BHs). In order to observe GWs directly, a new generation of GW detectors— Advanced LIGO (aLIGO: Abbott et al. 2016b), Advanced Virgo (aVirgo: Acernese et al. 2015), and KAGRA (Somiya 2012)—are being constructed. If the planned sensitivities are achieved, these GW detectors can detect GW signals from an NS–NS merger at a distance of 200 Mpc (Abadie et al. 2010). The GW detection rate is anticipated to be in the range of 0.4–400 events yr^{-1} for NS–NS merger (Abadie et al. 2010). Uncertainty in the above number primarily comes from the limit of our knowledge on the real number of NS binaries in a galaxy.

If a compact object merger contains one NS, a wide wavelength range of electromagnetic (EM) emission associated with the GWs is expected (Li & Paczynski 1998; Rosswog 2005; Metzger et al. 2010; Nakar & Piran 2011; Roberts et al. 2011; Metzger & Berger 2012;

Barnes & Kasen 2013; Hotokezaka et al. 2013; Tanaka & Hotokezaka 2013; Berger 2014; Tanaka et al. 2014). The EM emission would tell us important information about the nature of the GW event: its astrophysical origin, detailed localization, accurate distance, and the local environment of the event. The most promising optical–near-infrared emission from GW sources is radioactively powered emission, so-called "kilonova" or "macronova," associated with NS–NS or BH–NS mergers (Metzger & Berger 2012; Barnes & Kasen 2013; Tanaka et al. 2014). A strong tidal force induced by the merging process blows out the outer layer of the NS, and a wide solid angle outflow from the merger emits a wide range of EM emission due to radioactive decay of the ejecta; that is "kilonova." Neutron-rich ejecta of a kilonova produce a huge amount of r-process elements, and thus kilonova emission gives important clues to the long-standing mystery about the sites of cosmic r-process nucleosynthesis. Moreover, the luminosity and light curve of a kilonova would allow us to constrain the equation of state of the NS. To search for EM emission associated with GW events, we organized an EM follow-up observation network J-GEM (Japanese collaboration of Gravitational wave Electro-Magnetic follow-up: Morokuma et al. 2016) by utilizing optical, infrared, and radio telescopes in Japan.

The first direct detection of a GW was achieved by aLIGO on 2015 September 14 (Abbott et al. 2016a). aLIGO performed the first science run (O1) from 2015 September to 2016 January. Just before the regular operation of O1, aLIGO detected the GW at 2015 September 14 09:50:45 (UT) (Abbott et al. 2016a). The GW from this event, which was named GW150914, was emitted by a $36\,M_\odot$–$29\,M_\odot$ binary BH coalescence. While many electromagnetic (EM) follow-up observations were performed for GW150914 (Abbott et al. 2016d, 2016e; Ackermann et al. 2016; Evans et al. 2016a; Kasliwal et al. 2016; Lipunov et al. 2016; Morokuma et al. 2016; Serino et al. 2016; Smartt et al. 2016a; Soares-Santos et al. 2016; Troja et al. 2016), no clear EM counterpart was identified with those observations except for a possible detection of γ-ray emission by the Fermi Gamma-ray Burst Monitor (GBM: Connaughton et al. 2016). However, the Fermi GBM detection was not confirmed by INTEGRAL observations (Savchenko et al. 2016).

aLIGO detected another GW signal during O1. This event was detected at 03:38:53 (UT) on 2015 December 26 and was named GW151226. The false alarm probability of the event was estimated as $<10^{-7}$ ($>5\,\sigma$) and 3.5×10^{-6} ($4.5\,\sigma$: Abbott et al. 2016c). The GW was also attributed to a BH–BH binary merger with masses $14.2^{+8.3}_{-3.7}\,M_\odot$ and $7.5^{+2.3}_{-2.3}\,M_\odot$. The final BH mass was $20.8^{+6.1}_{-1.7}\,M_\odot$ and a gravitational energy of $\sim 1\,M_\odot$ was emitted as GWs. The distance to the event was 440^{+180}_{-190} Mpc (Abbott et al. 2016c).

Here, we report the EM counterpart search for GW151226 performed in the framework of J-GEM. We assume that the cosmological parameters h_0, Ω_m, and Ω_λ are 0.705, 0.27, and 0.73, respectively (Komatsu et al. 2011) in this paper, and all the photometric magnitudes presented are AB magnitudes.

2 Observations

We performed a wide-field survey and galaxy-targeted follow-up observations in and around the probability skymap of GW151226. The 90% credible area of the initial skymap created by the BAYESTAR algorithm (Singer et al. 2014) was $\sim$1400 deg^2 (LSC and Virgo Collaborations 2015). The final skymap was refined by the LALInference algorithm (Veitch et al. 2015) and the 90% area was finally 850 deg^2 (Abbott et al. 2016c). We also undertook integral field spectroscopy for an optical transient (OT) candidate reported by MASTER. The specifications of the instruments and telescopes we used for the follow-up observations are summarized in Morokuma et al. (2016).

2.1 Wide-field survey

We used three instruments for the wide-field survey: KWFC (Sako et al. 2012) on the 1.05 m Schmidt telescope at Kiso Observatory, HSC (Miyazaki et al. 2012) on the 8.2 m Subaru Telescope, and MOA-cam3 (Sako et al. 2008) on the 1.8 m MOA-II telescope at Mt John Observatory in New Zealand.

The KWFC survey observations were done in the r band on 2015 December 28 and 29, and 2016 January 1–6 (UT). The total area observed with KWFC was 778 deg^2, far off the Galactic plane. To perform an image subtraction with the archival SDSS (Sloan Digital Sky Survey: Alam et al. 2015) images, the high probability regions had to be avoided. Each field was observed typically twice or three times. The exposure time was 180 s each and the seeing was $2\farcs5$–$3\farcs0$ FWHM.

We carried out imaging follow-up observations with HSC in the first half nights of 2016 January 7, 13, and February 6 (UT). We observed an area of 63.5 deg^2 centered at $(\alpha, \delta) = (03^{\rm h}33^{\rm m}45^{\rm s}, +34^\circ57'14'')$ spanning over the highest probability region in the initial skymap (BAYESTAR) with 50 HSC fiducial pointings. The fiducial pointings were aligned on a Healpix (Gorski et al. 2005) grid with NSIDE = 64 (the corresponding grid size is 0.84 deg^2). To remove artifacts efficiently, we visited each fiducial pointing twice with a $2'$ offset. We observed the field in the i and z bands with an exposure time ranging from 45 s to 60 s for each pointing. On February 6, we first surveyed all the fields by single exposure, then observed

Table 1. Observing log of the wide-field survey observations.

Date (UT)	Instrument	mid-T* [d]	Area [deg^2]	Band	$m_{\rm lim}$† [AB mag]
2015-12-28	KWFC	2.43	176	r	19.2 ± 1.3
2015-12-29	KWFC	3.48	512	r	19.5 ± 0.3
2016-1-1	KWFC	6.59	48	r	17.1 ± 1.2
2016-1-2	KWFC	7.67	124	r	20.3 ± 0.2
2016-1-3	KWFC	8.70	56	r	20.1 ± 0.3
2016-1-4	KWFC	9.49	84	r	19.9 ± 0.3
2016-1-5	KWFC	10.36	40	r	19.8 ± 0.6
2016-1-6	KWFC	11.60	124	r	20.0 ± 0.2
2016-1-7	HSC	12.71	63.5	i, z	i: 24.3 ± 0.2, z: 23.5 ± 0.2
2016-1-13	HSC	18.17	63.5	i, z	i: 24.6 ± 0.2, z: 23.8 ± 0.2
2016-2-6	HSC	42.17	63.5	i, z	i: 24.4 ± 0.2, z: 23.8 ± 0.3
2016-3-8	MOA-cam3	73.31	55	MOA-red	18.2 ± 0.1
2016-3-9	MOA-cam3	74.31	11	MOA-red	17.3 ± 1.2
2016-3-10	MOA-cam3	75.35	117	MOA-red	18.2 ± 0.3
2016-3-11	MOA-cam3	76.30	15	MOA-red	18.2 ± 0.3

*Middle time of the observation in units of days after GW151226.
†Median value of 5 σ limiting magnitude and its range (1 σ) during one observation run.

the whole area again. The seeing ranged from 0.″5 to 1.″5 FWHM.

We also performed survey observations with MOA-cam3 for a part of the skymap in the southern hemisphere from 2016 March 8 to 11 (UT). The total area covered by the MOA-cam3 observations was 145 deg^2. The "MOA-Red" filter (Sako et al. 2008), which is a special filter dedicated to micro-lens survey with a wide range of transmission from 6200 Å to 8100 Å, was used. The exposure time per field was 120 s. The seeing was 1.″9–4.″5 FWHM.

Since the sky areas observed by the three instruments were not overlapped, the total area covered by the wide-field surveys was 986.5 deg^2. The integrated detection probabilities of the observed regions for the final skymap (LALInference) were 0.07, 0.09, and 0.13 for HSC, KWFC, and MOA-cam3, respectively. We thus covered a total of ∼29% of the probability skymap of GW151226.

The wide-field survey observations are summarized in table 1. The survey areas and the probability skymap of GW151226 are shown in figure 1. An enlarged map of the sky areas observed with HSC is shown in figure 2.

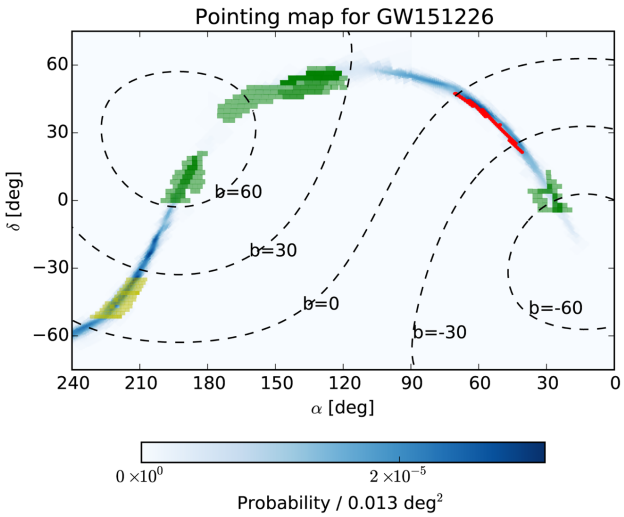

Fig. 1. Observed area of the wide-field surveys of the J-GEM follow-up observation of GW151226 overlaid on the probability skymap (dark blue scale). Green, red, and yellow colored regions represent the areas observed with KWFC, HSC, and MOA-cam3, respectively. (Color online)

2.2 Galaxy-targeted follow-ups

We performed targeted follow-up imaging observations from 2015 December 27 (UT). We used seven instruments on six telescopes for these observations: HOWPol (Kawabata et al. 2008) and HONIR (Akitaya et al. 2014) on the 1.5 m Kanata telescope, MINT on the 2 m Nayuta telescope, MITSuME (MITSuME-OAO: Kotani et al. 2005) on the 0.5 m telescope, OAO-WFC (Yanagisawa et al. 2014) on the 0.91 m telescope, MOA-cam3 on the 1.8 m MOA-II telescope, and SIRIUS (Nagayama et al. 2003) on the 1.4 m IRSF. We performed *R*-band observations with HOWPol and MITSuME, *I*-band observations with HOWPol, HONIR, and MINT, MOA-Red observations with MOA-cam3, *J*-band observations with OAO-WFC, and *J*-, *H*-, and *K*-band observations with SIRIUS.

We selected 309 nearby galaxies from GWGC (Gravitational Wave Galaxy Catalog: White et al. 2011) in the skymap regions whose detection probabilities were more than 0.0008. We divided the target galaxies into four target

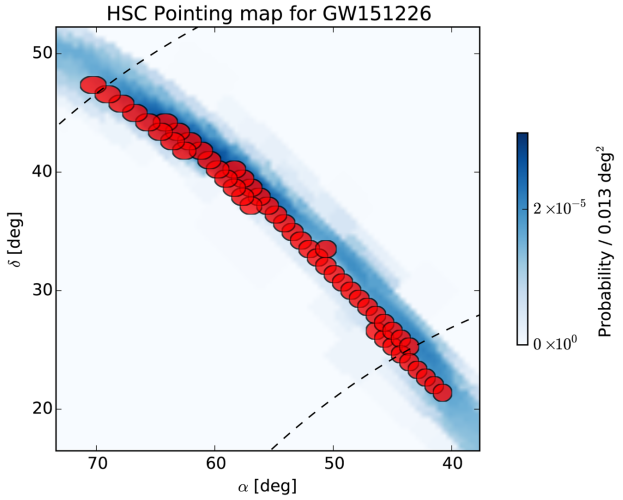

Fig. 2. Enlarged view of the HSC survey area. (Color online)

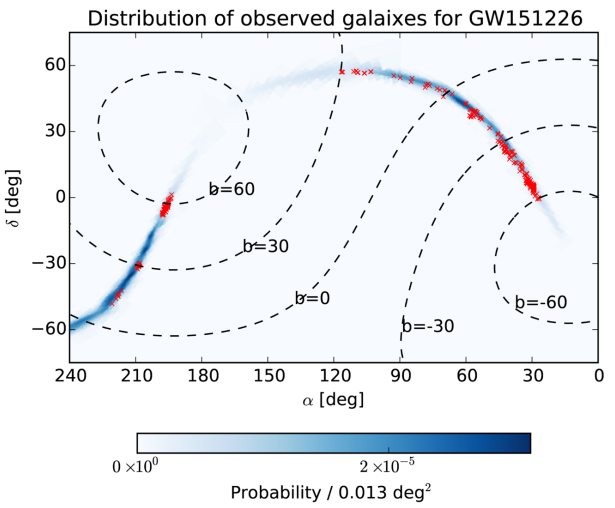

Fig. 3. Positions of the galaxies observed in the J-GEM follow-up observation of GW151226 (red points). (Color online)

groups. Groups 1 to 3 contained northern galaxies accessible from Japan. The number of galaxies in groups 1, 2, and 3 were 77, 76, and 77, respectively. Group 4 contained 79 southern galaxies. We allocated these groups to the above telescopes as target lists.

A summary of the targeted observations is shown in table 2. The net number of observed galaxies was 238. The spatial and distance distributions of the observed galaxies are shown in figures 3 and 4, respectively.

2.3 Spectroscopic follow-up

We carried out a spectroscopic observation of MASTER OT J020906.21+013800.1 (Lipunov et al. 2015) with a fiber-fed integral field spectrograph KOOLS-IFU attached to the 188 cm telescope at Okayama Astrophysical Observatory on 2015 December 28 (UT). The field of view of KOOLS-IFU is 1.″8 per fiber and 30″ in total. The wavelength range and spectral resolving power were 5020–8830 Å, and 600–850, respectively. The total exposure time was 3600 s.

3 Data reduction and results

3.1 Wide-field survey data

3.1.1 KWFC survey

Data reduction of the KWFC data was done using the standard data reduction pipeline developed for the Kiso Supernova Survey (KISS: Morokuma et al. 2014). The pipeline

Table 2. Average limiting magnitudes of the galaxy-targeted observations.

Date (UT)	Instruments	mid-T* [d]	N_{gal}†	exp-T [s]	m_{lim}‡ [AB]
2015-12-27	HOWPol	1.67	18	90	R: 17.9 ± 0.6, I: 18.3 ± 0.4
2015-12-28	MITSuME	2.46	61	540	R: 18.5 ± 0.4
	OAO-WFC	2.46	36	900	J: 18.3 ± 0.3
	MINT	2.47	37	540	I: 20.1 ± 0.5
	HONIR	2.49	51	120	I: 19.4 ± 0.5
	SIRIUS	2.78	10	360–580	J: 19.3 ± 0.4, H: 19.2 ± 0.4, K: 18.1 ± 0.4
2015-12-29	MITSuME	3.34	16	540	R: 18.5 ± 0.4
	MOA-cam3	3.45	10	120	MOA-red: 17.3 ± 0.7
	OAO-WFC	3.47	32	900	J: 16.4 ± 0.4
	HONIR	3.49	20	120	I: 19.7 ± 0.3
	MINT	3.53	38	540	I: 20.0 ± 0.6
2015-12-31	MOA-cam3	5.39	29	120	MOA-red: 18.4 ± 0.1
2016-01-04	MOA-cam3	9.40	24	120	MOA-red: 18.6 ± 0.2
2016-01-05	MOA-cam3	10.30	19	120	MOA-red: 18.2 ± 0.1

*Middle time of the observation in units of days after GW151226.
†Number of observed galaxies.
‡Median value of 5 σ limiting magnitude and its range (1 σ) during one observation run.

functions include bias subtraction, overscan subtraction, overscan trimming, flat-fielding, point spread function (PSF) size measurements, astrometry relative to the USNO-B1.0 catalog (Monet et al. 2003), zeropoint magnitude determination relative to the SDSS, image subtraction using the SDSS images, and detection of transient candidates in the subtracted images. The 5 σ limiting magnitudes of the KWFC observations ranged from 18.0 to 20.5, depending on the sky condition of the Kiso observatory.

The transient candidates detected in the subtracted images include not only astronomical objects but also non-astronomical artifacts, such as cosmic rays, residual of image subtraction due to imperfect image alignment or convolution (see, e.g., Bailey et al. 2007; Bloom et al. 2012). Moreover, astronomical objects include minor planets or variable stars in addition to extragalactic transients. Therefore, we first removed the transient candidates around the objects which are registered as stars in the SDSS catalog. This effectively removed both variable stars and artifacts around bright stars. Then, all the sources matching with the database of the Minor Planet Center were removed. Finally, the remaining objects were visually inspected to remove artifacts.

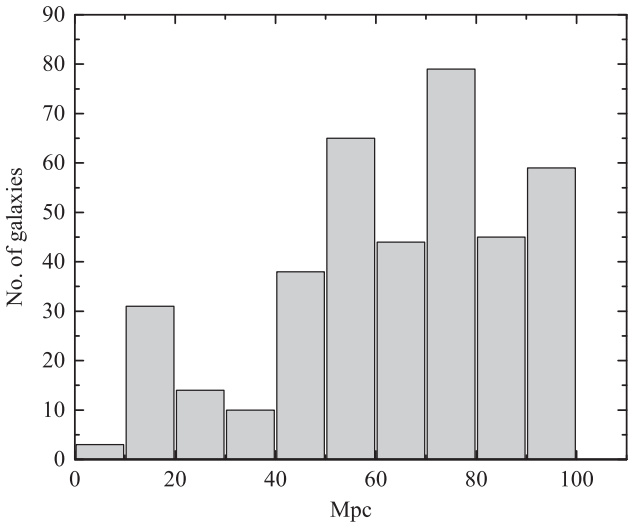

Fig. 4. Distance distribution of the observed galaxies. The distance limit (100 Mpc) of the galaxies is determined by GWGC.

As a result, we found 13 extragalactic transient candidates associated with galaxies. The candidates found with the KWFC are summarized in table 3. Nine out of 13 objects were detected more than twice in our survey. The other four objects (KISS15ah, KISS15ai, KISS16b, and KISS16c) were detected only once. Since KISS15ah and KISS16c were independently discovered by other groups (AT 2016bse and SN 2015bl, respectively), they must be genuine extragalactic transients. Although there is no independent discovery for KISS15ai and KISS16b, they are rather bright (16.6 and 19.6 mag, respectively), and unlikely to be minor planets which are not registered in the database of the Minor Planet Center.

In table 3, we show estimated absolute magnitudes of 13 transient candidates using spectroscopic and photometric redshifts. Except for KISS16f and KISS16b, the candidates were too bright for the expected kilonova emission (e.g., Tanaka et al. 2014), suggesting that they are supernovae (SNe). KISS16f and KISS16b were rather faint, but their host galaxies are located at $z = 0.012$ and 0.009964,

Table 3. Supernovae identified by the KWFC survey.

ID	RA [°]	Dec [°]	T_{obs}(UT)*	m_r [AB]	m_{lim}† [AB]	Host galaxy‡	spec-z§	photo-z	M_r‖ [AB]
KISS15ag	141.812070	51.480666	2015-12-28 13:40:48	17.5	19.30	SDSS J092715.01+512853.2	0.053	—	−19.4
KISS15ah	140.142947	50.696334	2015-12-29 12:57:36	18.0	19.17	SDSS J092034.44+504148.7	—	0.050 or 0.063	−19.1
KISS15ai	19.249817	−4.942760	2015-12-29 09:50:24	16.6	20.00	SDSS J011659.36−045629.0	—	0.03	−19.1
KISS15aj	137.536390	50.061012	2015-12-29 12:14:24	17.4	19.37	UGC 04812	0.0343	—	−18.6
KISS16a	126.579910	53.770297	2016-01-02 18:28:48	18.7	20.40	SDSS J082619.18+534610.5	0.042	—	−17.8
KISS16b	140.725655	46.534659	2016-01-02 20:52:48	19.6	20.26	KUG0919+467	0.009964	—	−13.7
KISS16c	134.969736	53.265282	2016-01-02 19:55:12	19.3	20.46	SDSS J085952.59+531547.7	0.093	—	−18.9
KISS16d	136.815119	52.762845	2016-01-02 19:55:12	19.5	20.46	SDSS J090715.76+524544.6	NA	0.1	−18.9
KISS16e	131.618647	53.758743	2016-01-02 18:57:36	19.8	20.18	SDSS J084628.73+534531.2	—	0.10 or 0.08	−18.4
KISS16f	140.055455	54.108287	2016-01-03 20:38:24	18.5	20.16	SDSS J092012.28+540628.1	0.012		−15.2
KISS16g#	186.709112	16.263777	2016-01-03 20:09:36	19.7	20.41	SDSS J122649.70+161546.7	—	0.55 or 0.26	−22.1
KISS16h	126.292102	56.706847	2016-01-06 19:12:00	19.0	20.52	SDSS J082510.12+564222.5	0.043	—	−17.5
KISS16i	185.281171	16.935903	2016-01-06 20:09:36	19.7	20.41	SDSS J122107.48+165607.1	—	0.1	−18.7

*Observation time (UT) of the events.

†5 σ limiting magnitude.

‡Closest galaxy in SDSS.

§All the spectral redshifts except for KISS15aj and KISS16b were taken from SDSS DR12 (Alam et al. 2015). The redshifts for KISS15aj and KISS16b were obtained from Fisher et al. (1995) and Falco et al. (1999), respectively.

‖When two values are given for photo-z, an average redshift is assumed.

#Identification of the host galaxy is uncertain. The host galaxy may be SDSS J122650.23+161618.2 ($z = 0.046$) located at about 29″ north, and then the absolute magnitude of the transient is −16.1 mag.

respectively, and thus they were not associated with GW151226. They are likely to be SNe after the peak brightness.

3.1.2 HSC survey

The HSC data were reduced using HSC pipeline version 4.0.1, which had been developed based on the LSST pipeline (Ivezic et al. 2008; Axelrod et al. 2010). The HSC pipeline provides packages for bias subtraction, flat-fielding, astrometry, mosaicing, warping, coadding, and image subtraction. The astrometry and photometry were made relative to the Pan-STARRS1 (PS1: Tonry et al. 2012; Schlafly et al. 2012; Magnier et al. 2013) with a 1.″5 (9 pixel) aperture diameter. The limiting magnitudes were estimated by randomly sampling $>10^5$ apertures.

The images taken on February 6 were used as reference images and were subtracted from the images taken on January 7 and 13. Here, we separately adopted images at two epochs on January 7, while images on January 13 were coadded. Point sources in the difference images were detected and measured with the HSC pipeline. Since there were many false detections, we screened the detected sources by the following selection procedure:

(1) In order to exclude false detections, we selected point sources detected in both the z-band difference images on January 7 at the same location with a signal-to-noise ratio of $>5\sigma$, ellipticity of >0.8, and FWHM of 0.″8–1.″3. In addition, a small residual of PSF subtraction from the sources ($<3\sigma$) was imposed.
(2) To select objects fading from January 7 to February 6, fluxes of sources in the two z-band difference images on January 7 were required to be positive.
(3) To exclude minor planets, first we estimated the maximum distance that an object could move during the interval between z- and i-band imaging observations. We found that it is $\sim$45″, assuming that the elongation in the z-band difference image was due to the movement of the object during the exposures. For the sources that survived selections 1 and 2, we checked the i-band difference images. If a source was not detected but another transient source was found at a distance of 0.″5–45″ in the i-band difference image, we omitted the source as a possible minor planet. We also checked the position of sources with Minor Planet Checker (MPChecker).[1]

After the above screening, 1256 candidates remained and were visually inspected. First, we removed clear artifacts from the candidate list by visual inspection. Then we identified and removed slowly moving objects which were thought to be distant minor planets not removed by criterion 3 above by carefully checking the images. Finally, 60 objects remained as extragalactic transient candidates.

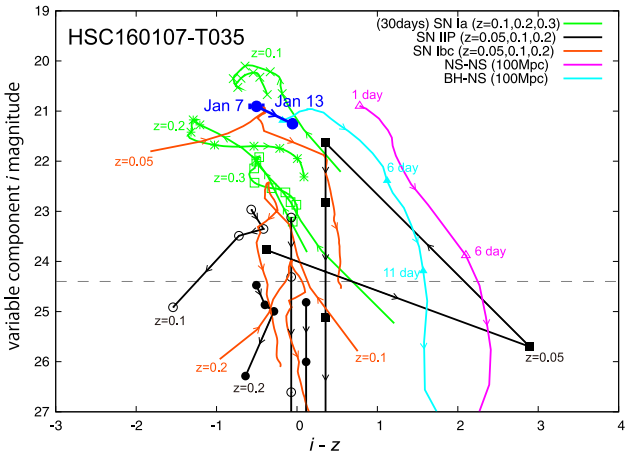

Fig. 5. Color-magnitude variation of the variable component of a transient candidate of the HSC follow-up survey of GW151226. Filled blue circles are the data of HSC160107-T035 taken from January 7 and 13 images after subtracting the February 6 image (Galactic extinction was corrected). Pink and light blue lines represent kilonova models of NS–NS merger and BH–NS merger of Tanaka et al. (2014)—see text. Green, black, and orange lines are the color-magnitude evolutions of variable components of SNe Type Ia, Type IIP, and Type Ibc, respectively. To derive the variable components of SNe, we subtracted the data 30 d after the explosions from the model light curves of SNe. (Color online)

The multicolor light curves of the candidates were derived with forced aperture photometry of the difference images with 1.″5 aperture diameter. We corrected for Galactic extinction using Schlegel, Finkbeiner, and Davis (1998).

We compared the color-magnitude time variations of the variable component of the transient candidates between January 7 and 13 with the color-magnitude evolutions of Type Ia, Ibc, and IIP SNe and kilonova emission, and classified the candidates (figure 5). For this comparison, we subtracted the brightnesses at 24 days and 30 days after the explosions from the model light curves of SNe and simulated the color-magnitude evolutions of the variable component of SNe. We adopted fiducial kilonova models of NS–NS merger with ejecta mass of 0.01 $M_\odot$ (model "APR4-1215" of Tanaka et al. 2014) and BH–NS merger with ejecta mass of 0.05 $M_\odot$ (model "H4Q3a75" of Tanaka et al. 2014).

By visual inspection and color-magnitude variation study, we found that two thirds of the HSC transients were probably SNe. One third of the HSC transients were located very close to the centers of the host galaxies and those time variabilities were not typical of SNe. We thus classified these sources as "active galactic nuclei (AGN)." No source whose color-magnitude variation was consistent with the kilonova

[1] ⟨http://www.minorplanetcenter.net/cgi-bin/checkmp.cgi⟩.

Table 4. Extragalactic transients identified by the HSC survey.

ID	RA [°]	Dec [°]	$E(B-V)$	$T_{\rm obs}(i)^*$	m_i [AB]	$T_{\rm obs}(z)^\dagger$	m_z [AB]	Type
HSC160107-T001	40.997379	22.369333	0.21	09:22:40	23.9	07:33:46	22.5	SN
HSC160107-T002	41.176235	22.611018	0.27	09:22:40	22.9	07:33:46	22.7	SN
HSC160107-T003	42.560811	23.350175	0.21	09:18:45	24.4	07:29:08	24.0	SN
HSC160107-T004	42.872344	22.315740	0.41	09:20:04	>24.2	07:30:41	22.2	SN
HSC160107-T005	43.455010	25.258338	0.12	09:12:10	>24.5	07:21:26	22.9	AGN
HSC160107-T006	43.507674	24.850162	0.12	09:11:31	>24.7	07:20:39	22.8	SN
HSC160107-T007	43.754581	23.637964	0.23	09:14:50	23.7	07:24:31	23.1	SN
HSC160107-T008	44.116261	24.054421	0.14	09:12:12	21.7	07:21:26	21.2	SN
HSC160107-T009	44.136838	25.945316	0.12	09:06:57	>24.0	07:15:12	21.7	SN
HSC160107-T010	44.364382	24.190641	0.13	09:11:32	24.0	07:20:39	22.8	AGN
HSC160107-T011	44.752975	26.107955	0.21	09:05:38	23.4	06:21:47	23.1	SN
HSC160107-T012	44.819914	24.395057	0.22	09:09:33	>23.9	07:18:20	22.2	AGN
HSC160107-T013	45.332537	25.263094	0.31	08:59:07	>24.7	05:21:51	23.0	AGN
HSC160107-T014	45.382080	24.835433	0.27	09:01:43	24.5	05:25:14	23.1	SN
HSC160107-T015	45.692939	26.530651	0.19	08:57:51	24.1	05:18:53	24.1	SN
HSC160107-T016	45.985724	27.425493	0.19	08:56:33	>25.0	05:18:28	22.3	AGN
HSC160107-T017	46.008330	25.975611	0.22	08:53:58	23.6	05:15:23	23.3	SN
HSC160107-T018	46.099802	27.108579	0.19	08:55:16	24.3	05:16:55	22.5	AGN
HSC160107-T019	46.346789	26.882343	0.21	08:55:16	22.5	05:16:55	22.4	SN
HSC160107-T020	46.462762	27.009164	0.21	08:56:20	21.6	05:18:12	21.2	SN
HSC160107-T021	46.830698	27.322635	0.21	08:53:58	>24.3	05:15:22	22.8	SN
HSC160107-T022	47.162617	28.111701	0.29	08:51:23	23.5	05:12:15	23.1	SN
HSC160107-T023	47.180281	28.363844	0.25	08:48:49	24.2	05:09:08	23.9	SN
HSC160107-T024	47.648348	28.246272	0.49	08:48:49	24.0	05:09:08	22.6	SN
HSC160107-T025	47.734609	28.924534	0.37	08:47:30	23.7	05:07:35	22.8	SN
HSC160107-T026	47.762266	29.189132	0.29	08:46:51	>24.3	05:06:49	22.7	SN
HSC160107-T027	48.584401	30.219543	0.37	08:41:28	>24.8	05:45:30	23.6	AGN
HSC160107-T028	48.878845	30.786932	0.37	08:37:52	21.7	07:11:24	21.5	SN
HSC160107-T029	50.365169	33.849423	0.24	08:40:38	21.0	04:59:49	20.8	SN
HSC160107-T030	50.453222	32.469045	0.41	08:28:22	>24.3	07:00:39	23.3	SN
HSC160107-T031	50.621347	32.624719	0.38	08:27:00	22.7	06:59:05	22.2	AGN
HSC160107-T032	50.830253	32.696495	0.40	08:25:38	>24.6	06:57:32	22.6	AGN
HSC160107-T033	50.892772	32.243608	0.38	08:27:00	23.1	06:59:05	23.1	SN
HSC160107-T034	51.672064	33.625310	0.27	08:18:53	23.0	06:50:19	22.6	AGN
HSC160107-T035	52.595560	35.179117	0.29	08:10:29	21.4	06:41:00	21.7	SN
HSC160107-T036	53.315983	35.731965	0.27	08:11:54	>24.7	06:42:33	23.6	SN
HSC160107-T037	53.909867	35.092927	0.34	08:11:54	23.9	06:42:33	23.5	SN
HSC160107-T038	54.092770	35.448804	0.30	08:11:54	>24.3	06:42:33	22.2	SN
HSC160107-T039	54.585872	37.015130	0.52	08:22:12	>24.1	06:53:56	22.4	SN
HSC160107-T040	54.912712	36.394118	0.44	08:22:12	>23.8	06:53:56	20.9	AGN
HSC160107-T041	55.370525	37.555876	0.44	08:52:46	>24.6	06:36:00	23.3	AGN
HSC160107-T042	55.632338	36.242112	0.49	08:22:12	>24.4	06:53:56	22.9	SN
HSC160107-T043	56.537885	38.800077	0.32	09:31:06	23.2	05:35:10	24.0	AGN
HSC160107-T044	56.639089	36.644814	0.40	09:33:41	23.2	05:38:16	22.8	SN
HSC160107-T045	56.898156	36.857295	0.36	09:33:41	22.1	05:38:16	22.7	AGN
HSC160107-T046	57.003385	36.936598	0.34	09:33:41	22.5	05:38:16	22.6	SN
HSC160107-T047	57.024877	36.695131	0.38	09:33:41	21.2	05:38:16	21.9	SN
HSC160107-T048	58.172853	37.840891	0.95	09:38:58	23.5	05:44:25	22.8	SN
HSC160107-T049	60.477172	39.860675	0.83	09:49:23	22.3	05:56:43	21.6	AGN
HSC160107-T050	62.176935	42.152778	0.58	09:58:26	23.4	06:07:32	23.6	SN
HSC160107-T051	63.477258	41.424544	0.73	09:59:44	23.2	06:09:05	>23.2	SN
HSC160107-T052	64.308645	42.773320	0.78	10:07:36	24.7	06:18:34	22.5	AGN
HSC160107-T053	64.875372	43.850244	0.79	10:10:14	25.1	06:21:41	23.0	AGN
HSC160107-T054	65.638499	43.614708	0.70	10:12:52	22.3	06:24:49	22.4	SN

Table 4 (Continued)

ID	RA [°]	Dec [°]	$E(B-V)$	$T_{obs}(i)$*	m_i [AB]	$T_{obs}(z)$†	m_z [AB]	Type
HSC160107-T055	66.332247	44.279330	0.80	10:14:11	22.2	06:26:22	21.5	SN
HSC160107-T056	67.121767	45.254756	1.48	10:17:29	>24.3	06:29:26	20.7	AGN
HSC160107-T057	67.213427	45.250006	1.52	10:16:50	23.4	06:29:26	22.5	SN
HSC160107-T058	69.108532	46.036008	1.78	10:20:46	22.8	06:34:05	21.8	SN
HSC160107-T059	69.776861	46.009513	1.55	10:20:46	>24.5	06:34:05	22.2	SN
HSC160107-T060	69.983965	47.715348	1.40	10:23:25	22.8	06:37:13	21.2	AGN

*Observation time (UT) in *i* band on 2016 January 7.
†Observation time (UT) in *z* band on 2016 January 7.

models was identified by the above procedure. The extragalactic transient candidates found by the HSC survey are summarized in table 4.

Morokuma et al. (2008) derived the number densities of various transient objects as a function of time interval of i'-band observations from Subaru Suprime-Cam data in the Subaru/XMM-Newton Deep Field (Furusawa et al. 2008). According to figure 12 of Morokuma et al. (2008), the number density of extragalactic transients (SNe + AGNs) brighter than the variable component i' magnitude i'_{vari} of 25 mag with 30 days interval observations is ∼30. The variable component *i*-band limiting magnitude and the number density of the extragalactic transients in our work are ∼24 mag (see table 4) and ∼1 deg^{-2}, respectively. Scaling the number density of Morokuma et al. (2008) using their figure 13, we estimate that it would be 3–4 deg^{-2} for the limiting magnitude $i'_{vari} \sim 24$ mag. This is a few times higher than the value of our observation. Part of this discrepancy would come from our detection strategy. We detected the transients based on *z*-band observation, thus we could systematically undercount blue transients. In addition, since the Galactic latitude *b* of the HSC observation field is less than ∼30° (see figure 1), a large fraction of the field suffered from Galactic extinction [typical color excess $E(B-V)$ is ∼0.3–0.7; see table 4]. Considering these factors, we judge that our observation is roughly consistent with Morokuma et al. (2008).

3.1.3 MOA-II survey

The data of MOA-II were reduced in the standard manner of CCD data reduction using IRAF. Astrometry of the data was done using Astrometry.net (Lang 2009). Then point source candidates were extracted with SExtractor (Bertin & Arnouts 1996). After excluding known stars using the USNO-B1.0 catalog, we omitted the candidates whose brightness profiles were not consistent with PSF by profile fitting using IRAF task ALLSTAR. We visually inspected the remaining 2953 candidates and selected 39 sources as transient object candidates. Then we checked 2MASS (Skrutskie et al. 2006) and WISE (Wright et al. 2010) images and found that 33 of the 39 candidates were 2MASS sources and one was a WISE source. Using MPChecker, we found that three candidates were asteroids. One of the candidates was a known supernova, PSN J14102342-4318437.

After all selections, one candidate with ∼18.0 mag located at $(\alpha, \delta) = (14^h44^m41^s.06, -44°4'38''.4)$ remained. This source did not seem to be associated with bright galaxies. We observed this source twice with an interval of 180 s on 2016 March 10 and did not detect significant motion between the two exposures. It completely disappeared at the third observation, performed at the end of 2016 August. Though we cannot exclude the possibility that this source is an extragalactic transient, we think that the most plausible explanation is a minor planet not cataloged in MPChecker.

In the above processing, faint objects embedded in galaxies could be systematically lost. To detect such sources, we selected 2143 galaxies between 250 and 620 Mpc in the observed fields using GLADE (Galaxy List for the Advanced Detector Era).[2] We found 549 point sources within 5″ around these galaxies. Compared to DSS images, we found all the sources were known objects.

3.2 Galaxy-targeted follow-up data

The data reduction of the instruments used for the galaxy targeted observations—HOWPol, HONIR, MINT, MITSuME, MOA-II, OAO-WFC, and SIRIUS—was made in a standard manner: overscan correction, bias and dark subtraction, and flat-fielding. Then multiple exposure frames were coadded. Photometric calibration of the optical data was done by comparing the fluxes of the field stars with those listed in the SDSS or GSC2.3 (Guide Star Catalog version 2.3). For the near-infrared band data calibration, we used the 2MASS point source catalog (PSC: Skrutskie

[2] ⟨http://aquarius.elte.hu/glade⟩.

et al. 2006). The observed galaxies and the limiting magnitudes of our observations are listed in figure 1 of the online supplementary data (e-table 1).

We searched for transient point sources in the observed frames taken with the above instruments by comparing them with DSS red frames for the R and I bands, and with 2MASS PSC for near-infrared bands. We found transient candidates in I-band frames of the galaxies PGC1202981 and UGC 1410 taken with HONIR on 2015 December 28. However, the former was a Galactic variable star and the latter was a known minor planet. We also found a possible transient candidate close to the nucleus of PGC1021744 in a J-band image taken with OAO-WFC on 2015 December 28. Since the source was slightly fainter than the $5\,\sigma$ limiting magnitude of the image ($\sim$17.2 mag), the detection was quite marginal. We made a follow-up observation of this object with OAO-WFC the next night. The limiting magnitude of the observation reached 19.2 mag in the J band with an exposure time of 2700 s, but no point source was found at the same position. We thus could not confirm whether the source was a real astronomical transient.

As a conclusion, no extragalactic transient object was found with our galaxy-targeted follow-up of GW151226.

3.3 Spectroscopic follow-up data

The target of the spectroscopy, MASTER OT J020906.21+013800.1, was reported at an unfiltered magnitude of 18.3 in the skymap area of GW151226 on 2015 December 27 (UT) and reported to be brightening (Lipunov et al. 2015). Our integral field spectroscopy found no significant signal from the OT candidate. Given that the radial intensity profile of the object is Gaussian with FWHM of 3″, $\sim$40% of the object flux falls in three fibers. The $5\,\sigma$ limiting magnitude was 17.4 at 7400 Å. It is noted that the observations with the 3.6 m TNG starting on 2015 December 28.8247 (UT) also did not find any evidence for the OT with an upper limit of $r = 21.0$ mag (D'Avanzo et al. 2015). They detected the emission from a faint galaxy at a redshift of $\sim$0.034 at the position of the OT (D'Avanzo et al. 2015).

4 Discussion and conclusion

No optical or near-infrared counterpart of the gravitational wave event GW151226 was identified by the follow-up observations under the J-GEM collaboration. Other teams' attempts to find EM counterparts associated with this event also failed (Adriani et al. 2016; Cowperthwaite et al. 2016; Evans et al. 2016b; Racusin et al. 2016; Smartt et al. 2016b). We found 13 SNe candidates in the KWFC survey data, and 60 extragalactic transients in the HSC survey data. About two thirds of the HSC transients were probably SNe, and the remaining one third were classified as possible AGNs. There was no source which showed the color-magnitude variation consistent with current kilonova models in our dataset. We thus conclude that this work did not find clear candidates for an EM counterpart of the gravitational wave source.

Both of the GW events, GW150914 and GW151226, detected by aLIGO were BH–BH mergers. Inspired by the possible detection of a γ-ray emission associated with GW150914 by the Fermi satellite (Connaughton et al. 2016), several physical mechanisms for EM emission from a BH–BH merger event have been proposed (Morsony et al. 2016; Perna et al. 2016; Yamazaki et al. 2016). However, all of those theoretical works have difficulties in producing strong EM emission from a BH–BH merger. In addition, questions have been raised concerning the reality of the γ-ray detection by Fermi both from theoretical side (Lyutikov 2016; Zhang et al. 2016) and observational and data analysis side (Greiner et al. 2016; Savchenko et al. 2016; Xiong 2016). Thus there is still no observational evidence with a concrete theoretical background for EM emission from BH–BH merger. In other words, the key ingredient for detection of an EM counterpart associated with a GW is whether it contains a neutron star. Hence the information of the chirp mass of a GW event is crucial for EM follow-up observations. When the chirp mass and distance estimation of a GW event is distributed, EM follow-up teams will be able to make effective observation plans with their available facilities (Singer et al. 2016).

For considering future observation strategies, we summarize the observation epochs and the limiting magnitudes of the J-GEM follow-up of GW151226 in figure 6. The limiting magnitudes of the R, r, I, i, and MOA-red bands taken with HOWPol, HONIR, MINT, MITSuME, MOA-cam3, KWFC, and HSC are plotted with theoretical i-band light curves of kilonovae (Tanaka et al. 2014; Tanaka 2016). Our early observations with the small and mid-sized telescopes reached the depth of $\sim$20 mag in the optical red bands. The KWFC data around 6–8 d after the GW event were as deep as $\sim$20.5 mag. The deepest data taken with HSC reached down to $\sim$24 mag in the i band at 12 d after GW151226. According to the theoretical light curves in figure 6, the depth of our early galaxy-targeted observations reached the detection threshold of kilonova emission from a BH–NS merger within a distance of $\sim$50–100 Mpc. The late KWFC observations at around 7 d after the GW could follow the candidate. The deep HSC observations could follow the light curve of the candidate at most one month after the event.

However, if the event were an NS–NS merger, the story would be completely changed. The kilonova emission for

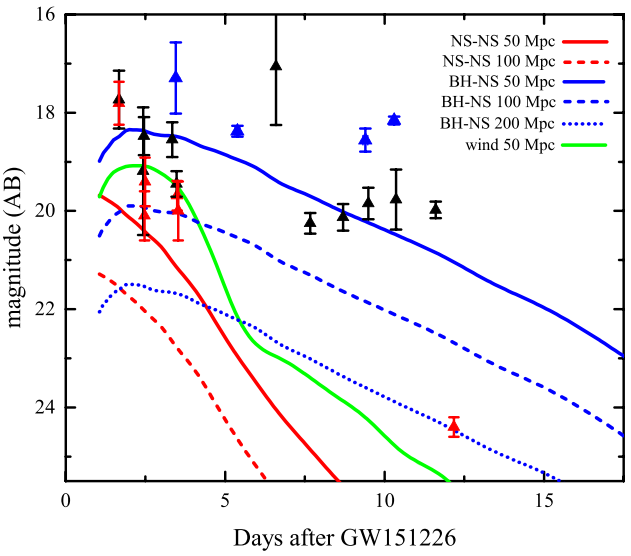

Fig. 6. Limiting magnitudes of the J-GEM observations of GW151226 and kilonova light curves. Filled triangles represent median 5 σ limiting magnitudes, and the *y*-axis error bars show the range of variation of the limiting magnitudes in the observed data sets. Black, red, and blue colors represent the *R* (*r* for KWFC) band, *I* (*i* for HSC) band, and MOA-red band, respectively. The theoretical *i*-band light curves of NS–NS merger (APR4-1215 of Tanaka et al. 2014) and BH–NS merger (H4Q3a75 of Tanaka et al. 2014) are shown as red and blue lines, respectively. The green line shows the *i*-band light curve of a model of the emission from shocked wind from NS–NS merger with ejecta mass of 0.03 $M_{\odot}$ (Tanaka 2016). Solid, dashed, and dotted lines correspond to event distances of 50 Mpc, 100 Mpc, and 200 Mpc, respectively. (Color online)

NS–NS merger is too faint to detect with our observations. Even if the event distance is 50 Mpc, the maximum magnitude of the optical emission would be much fainter than ∼19 mag at 1 d after the event. Only HSC could detect the optical emission from a kilonova at a distance of 50–100 Mpc if the follow-up observation with HSC was performed within ∼5 d after the event.

HSC has the capability of surveying over ∼60 deg^2 with two colors, *i* and *z* bands, with a limiting magnitude of ∼24 mag within a half night. Figure 6 shows that quick (<3 d) follow-up observations with HSC can detect the optical emission of a kilonova induced by an NS–NS merger at a distance of ∼200 Mpc. For BH–NS mergers, a relatively slow start of the observation is acceptable. The kilonova EM emission from BH–NS merger at a distance of 400 Mpc would be detectable by HSC even after 10 d from the GW event. When aVirgo goes into regular operation and joint observation by aLIGO and aVirgo starts, the 90% credible area for GW detection would become smaller than ∼50 deg^2, depending on the signal-to-noise ratio of the event (Singer et al. 2014). This size of area matches very well the area covered by half-night observation by HSC, and thus detection of EM emission from a kilonova is greatly anticipated.

Acknowledgements

This work makes use of software developed for the Large Synoptic Survey Telescope. We thank the LSST Project for making their code available as free software at http://dm.lsstcorp.org. The Pan-STARRS1 Surveys (PS1) have been made possible through contributions of the Institute for Astronomy, the University of Hawaii, the Pan-STARRS Project Office, the Max-Planck Society and its participating institutes, the Max Planck Institute for Astronomy, Heidelberg and the Max Planck Institute for Extraterrestrial Physics, Garching, The Johns Hopkins University, Durham University, the University of Edinburgh, Queen's University Belfast, the Harvard-Smithsonian Center for Astrophysics, the Las Cumbres Observatory Global Telescope Network Incorporated, the National Central University of Taiwan, the Space Telescope Science Institute, the National Aeronautics and Space Administration under Grant No. NNX08AR22G issued through the Planetary Science Division of the NASA Science Mission Directorate, the National Science Foundation under Grant No. AST-1238877, the University of Maryland, and Eotvos Lorand University (ELTE). This research has made use of the NASA/IPAC Extragalactic Database (NED) which is operated by the Jet Propulsion Laboratory, California Institute of Technology, under contract with the National Aeronautics and Space Administration. This work was supported by MEXT Grant-in-Aid for Scientific Research on Innovative Areas "New Developments in Astrophysics Through Multi-Messenger Observations of Gravitational Wave Sources" (JP24103003), JSPS KAKENHI Grant Numbers JP26800103 and JP15H02069, and the research grant program of the Toyota Foundation (D11-R-0830).

Supporting information

Additional supporting information may be found in the online version of this article: E-table 1.

References

Abadie, J., et al. 2010, Class. Quant. Grav., 27, 173001
Abbott, B. P., et al. 2016a, Phys. Rev. Lett., 116, 061102
Abbott, B. P., et al. 2016b, Phys. Rev. Lett., 116, 131103
Abbott, B. P., et al. 2016c, Phys. Rev. Lett., 116, 241103
Abbott, B. P., et al. 2016d, ApJ, 826, L13
Abbott, B. P., et al. 2016e, ApJS, 225, 8
Acernese, E., et al. 2015, Class. Quant. Grav., 32, 024001
Ackermann, M., et al. 2016, ApJ, 823, L2
Adriani, O., et al. 2016, ApJ, 829, L20
Akitaya, H., et al. 2014, Proc. SPIE, 9147, 91474O
Alam, S., et al. 2015, ApJS, 219, 12
Axelrod, T., Kantor, J., Lupton, R. H., & Pierfederici, F. 2010, Proc. SPIE, 7740, 774015
Bailey, S., Aragon, C., Romano, R., Thomas, R. C., Weaver, B. A., & Wong, D. 2007, ApJ, 665, 1246
Barnes, J., & Kasen, D. 2013, ApJ, 775, 18
Berger, E. 2014, ARA&A, 52, 43
Bertin, E., & Arnouts, S. 1996, A&AS, 117, 393
Bloom, J. S., et al. 2012, PASP, 124, 1175
Connaughton, V., et al. 2016, ApJ, 826, L6
Cowperthwaite, P. S., et al. 2016, ApJ, 826, 29
D'Avanzo, P., et al. 2015, GCN Circ., 18775

Evans, P. A., et al. 2016a, MNRAS, 460, 40
Evans, P. A., et al. 2016b, MNRAS, 462, 1591
Falco, E. E., et al. 1999, PASP, 111, 438
Fisher, K. B., Huchra, J. P., Strauss, M. A., Davis, M., Yahil, A., & Schlegel, D. 1995, ApJS, 100, 69
Furusawa, H., et al. 2008, ApJS, 176, 1
Górski, K. M., Hivon, E., Banday, A. J., Wandelt, B. D., Hansen, F. K., Reinecke, M., & Bartelmann, M. 2005, ApJ, 622, 759
Greiner, J., Burgess, J. M., Savchenko, V., & Yu, H.-F. 2016, ApJ, 827, L38
Hotokezaka, K., Kiuchi, K., Kyutoku, K., Muranushi, T., Sekiguchi, Y., Shibata, M., & Taniguchi, K. 2013, Phys. Rev. D, 87, 024001
Ivezic, Z., et al. 2008, arXiv:0805.2366
Kasliwal, M. M., et al. 2016, ApJ, 824, 24
Kawabata, K. S., et al. 2008, Proc. SPIE, 7014, 70144L
Komatsu, E., et al. 2011, ApJS, 192, 18
Kotani, T., et al. 2005, Nuovo Cim. C, 28, 755
Lang D. 2009, Ph.D. thesis, University of Toronto
Li, L.-X., & Paczynski, B. 1998, ApJ, 507, L59
LIGO Scientific Collaboration and Virgo Collaboration 2015, GCN Circ., 18728
Lipunov, V., et al. 2015, GCN Circ., 18729
Lipunov, V. M., et al. 2016, arXiv:1605.01607
Lyutikov, M. 2016, arXiv:1602.07352
Magnier, E. A., et al. 2013, ApJS, 205, 20
Metzger, B. D., et al. 2010, MNRAS, 406, 2650
Metzger, B. D., & Berger, E. 2012, ApJ, 746, 48
Miyazaki, S., et al. 2012, Proc. SPIE, 8446, 84460Z
Monet, D. G., et al. 2003, AJ, 125, 984
Morokuma, T., et al. 2008, ApJ, 676, 163
Morokuma, T., et al. 2014, PASJ, 66, 114
Morokuma, T., et al. 2016, PASJ, 68, L9
Morsony, B. J., Workman, J., Jared, G., & Ryan, D. M. 2016, ApJ, 825, 24
Nagayama, T., et al. 2003, Proc. SPIE, 4841, 459
Nakar, E., & Piran, T. 2011, Nature, 478, 82
Perna, R., Lazzati, D., & Giacomazzo, B. 2016, ApJ, 821, L18
Racusin, J. L., et al. 2016, arXiv:1606.04901
Roberts, L. F., Kasen, D., Lee, W. H., & Ramirez-Ruiz, E. 2011, ApJ, 736, L21
Rosswog, S. 2005, ApJ, 634, 1202
Sako, S., et al. 2008, Exp. Astron., 22, 51
Sako, S., et al. 2012, Proc. SPIE, 8446, 844673
Savchenko, V., et al. 2016, ApJ, 820, L36
Schlafly, E. F., et al. 2012, ApJ, 756, 158
Schlegel, D. J., Finkbeiner, D. P., & Davis, M. 1998, ApJ, 500, 525
Serino, M., et al. 2016, GCN Circ., 19013
Singer, L. P., et al. 2014, ApJ, 795, 105
Singer, L. P., et al. 2016, ApJ, 829, L15
Skrutckie, M. F., et al. 2006, AJ, 131, 1163
Smartt, S. J., et al. 2016a, MNRAS, 462, 4094
Smartt, S. J., et al. 2016b, ApJ, 827, L40
Soares-Santos, M., et al. 2016, ApJ, 823, L33
Somiya, K. 2012, Class. Quant. Grav., 29, 124007
Tanaka, M. 2016, Adv. Astron., 2016, 634197
Tanaka, M., & Hotokezaka, K. 2013, ApJ, 775, 113
Tanaka, M., Hotokezaka, K., Kyutoku, K., Wanajo, S., Kiuchi, K., Sekiguchi, Y., & Shibata, M. 2014, ApJ, 780, 31
Tonry, J. L., et al. 2012, ApJ, 750, 99
Troja, E., Read, A. M., Tiengo, A., & Salvaterra, R. 2016, ApJ, 822, L8
Veitch, J., et al. 2015, Phys. Rev. D, 91, 042003
White, D. J., Daw, E. L., & Dhillon, V. S. 2011, Class. Quant. Grav., 28, 085016
Wright, E. L., et al. 2010, AJ, 140, 1868
Xiong, S. 2016, arXiv:1605.05447
Yamazaki, R., Asano, K., & Ohira, Y. 2016, PTEP, 2016, 051E01
Yanagisawa, K., et al. 2014, Proc. SPIE, 9147, 91476D
Zhang, S.-N., Liu, Y., Yi, S., Dai, Z., & Huang, C. 2016, arXiv:1604.02537